Classification: Cell Biology, Biochemistry, Biophysics and Computational Biology

Title: Septin assemblies form by diffusion-driven annealing on membranes

Authors: Andrew A. Bridges[a,b], Huaiying Zhang[a,b], Shalin Mehta[b], Patricia Occhipinti[a], Tomomi Tani[b], and Amy S. Gladfelter[a,b]

Affiliations:

[a]Department of Biological Sciences, Dartmouth College, 78 College Street, Hanover, NH 03755

[b]Cellular Dynamics Program, Marine Biological Laboratory, 7 MBL Street, Woods Hole, MA 02543

Correspondence to Amy S. Gladfelter: 78 College Street, Hanover, NH 03755. 603-646-8706. amy.gladfelter@dartmouth.edu

Key words:

Cytoskeleton, septin, plasma membrane, diffusion, annealing

Abstract

Septins assemble into filaments and higher-order structures that act as scaffolds for diverse cell functions including cytokinesis, cell polarity, and membrane remodeling. Despite their conserved role in cell organization, little is known about how septin filaments elongate and are knit together into higher-order assemblies. Using fluorescence correlation spectroscopy (FCS), we determined that cytosolic septins are in small complexes suggesting that septin filaments are not formed in the cytosol. When the plasma membrane of live cells is monitored by total internal reflection fluorescence (TIRF) microscopy, we see that septin complexes of variable size diffuse in two dimensions. Diffusing septin complexes collide and make end-on associations to form elongated filaments and higher-order structures, an assembly process we call annealing. Septin assembly by annealing can be reconstituted in vitro on supported lipid bilayers with purified septin complexes. Using the reconstitution assay, we show that septin filaments are highly flexible, grow only from free filament ends and do not exchange subunits in the middle of filaments. This work shows for the first time that annealing is an intrinsic property of septins in the presence of membranes and demonstrates that cells exploit this mechanism to build large septin assemblies.

Significance Statement

The mechanisms and location of polymerization and disassembly direct the function of cytoskeletal proteins. Septins are far less understood than other cytoskeletal elements such as actin and microtubules, yet they have a conserved function acting as scaffolds at cell membranes and are implicated in cancers, neurodegenerative diseases, and microbial pathogenesis. We have defined a key role of the membrane in directing septin filament formation in live cells and reconstituted dynamic septin polymerization using purified components. We find that septins grow into filaments and form higher order structures by diffusing, colliding and annealing on the plasma membrane. This work is important because it defines for the first time the basic steps of polymerization and construction of higher-order assemblies of septin proteins.

\body

Introduction

Septin filaments form rings, bars and gauzes that serve as a scaffold at cell division sites, act to retract blebbed regions of membrane and restrict diffusion between cell compartments (1-4). Septin function is required for cell division and viability in many eukaryotes while misregulation is associated with cancers and neurodegenerative disorders (5-8). Furthermore, septins mediate entry of both bacterial and fungal pathogens into host cells (9-11). In vivo, septin assembly is restricted both in time and space through local activation of small GTPases such as Cdc42. Localized signaling leads to higher-order septin structures forming closely apposed to the plasma membrane at the plane of division, sites of polarity, and curved membranes (10, 12-14). Notably, eukaryotic cells of different geometries build higher-order septin assemblies of various shapes, sizes and functions (4, 15, 16). Though septins are critical for spatial organization of cell plasma membranes, their assembly and disassembly dynamics are not understood (15).

Electron microscopy (EM) studies of recombinant and immunoprecipitated *Saccharomyces cerevisiae* septins have shown that septins form non-polar hetero-octameric rod-shaped complexes in high salt buffers (>300 mM) and elongated filaments when dialyzed into low salt buffers (<100 mM) (17, 18). Structural analyses of worm and mammalian septins have revealed that the heteromeric, rod-shaped complex is conserved (19-21). Thus, septin rods characterized to date contain two copies of each septin subunit assembled into a non-polar, heteromeric complex (Fig.S1). Association of pure septin proteins with phosphoinositide-containing membrane

monolayers placed on EM grids can promote the assembly of septin filaments in otherwise non-permissive conditions such as high salt or the presence of mutant septins in the complex (22). A polybasic region in the N-terminus of septin proteins as well as other surfaces of the septin protein have been proposed to be the basis for septin association with phosphoinositides, however the functional role of membranes in filament formation is not yet known (22-24).

Previous work has defined a possible starting state of assembly (the rod) and endpoint (filaments and gauzes), however there is nothing known about how filaments elongate either in vivo or in vitro. Do septin filaments extend by step-wise addition of rods? Does addition occur from both ends of the filament? Can subunits be added in the middle and/or sides of a filament? Do septin filaments grow in the cytosol or on plasma membranes? Thus, it is still not known where filaments form in vivo, how filaments elongate and how filaments are brought together to construct higher-order assemblies.

The goal of this study was to identify the locations and mechanism of septin filament polymerization. Using fluorescence correlation spectroscopy (FCS) we observed that cytosolic septins are likely rods, not monomers or filaments. Using total internal reflection fluorescence (TIRF) microscopy we found septins form short filaments on the plasma membrane and then long filaments and higher-order assemblies grow when filaments merge. We have called the process of short filaments coming together “annealing” as this has previously been described for F-actin in vitro (25). We reconstituted septin assembly using purified proteins and supported lipid bilayers and found that annealing is an intrinsic property of septins that occurs at very low protein

concentrations in the presence of a supported phospholipid bilayer. Our results suggest that the plasma membrane concentrates septins and provides a platform for two-dimensional diffusion that promotes polymerization.

Results

Septins are in small, oligomeric complexes in cytosol

To determine how and where septins transition from monomers to filaments, we observed septins in the cytosol of three different fungal organisms: *S. pombe*, *S. cerevisae*, and *A. gossyppii*. These three systems have distinct cell morphologies and cell cycle controls influencing septin assembly and function. In all three systems, a septin was tagged with GFP at the native locus and expressed as the sole copy of the gene so as to monitor endogenous levels and enable quantitative analysis of fluorescence intensity. To examine composition and properties of septin complexes in the cytoplasm, fluctuations in fluorescence intensity were monitored and autocorrelated using fluorescence correlation spectroscopy (FCS). The cytoplasmic concentration of fluorescently-labeled septins was measured to be 100-200 nM, which is on the order of previous estimates in *S. pombe* using different approaches (Fig. S2A) (26).

We expected to observe cytosolic septins behaving as if they were in one of three states: as individual proteins, as rod complexes with two copies of each septin, or as filaments (Fig. S1). Molecular brightness measurements by FCS indicated that septins in the cytosol of all three model systems are in complexes containing 1-2 fluorescently-labeled molecules (Fig. *1A* and Fig S2*B-D*). Importantly, similar molecular brightness values were measured regardless of which septin family member was

tagged with GFP (Spn1/Cdc3 in *S. pombe*, Cdc11 in *A. gossypii* and Cdc11 or Cdc3 in *S. cerevisiae;* Fig. *1A* and Figs S2*B*-*D*). We suspect that in some cases a single molecule rather than two fluorescent molecules is detected because a subset of rods are in intermediate states of assembly, disassembly or both chromophores in the complex have not fully matured. Furthermore, cytoplasmic septins diffused at 0.67 +/- 0.29 $\mu m^2/s$ (*S. pombe*) which is much slower than cytoplasmic mEGFP alone which was 25.80 +/- 7.97 $\mu m^2/s$. This diffusion behavior is consistent with a complex that is likely larger in size than a single septin protein (Fig. *1A* and Figs S2B-D). The reproducible detection of septin complexes with 1-2 fluorescent molecules and the slow diffusion of these complexes relative to mEGFP suggest septins are predominantly in heteromeric rods in the cytosol rather than in monomers or filaments.

Septins elongate by annealing on plasma membranes

We next assessed the properties of septins at the plasma membrane of living cells using TIRF microscopy. Septins were found to diffuse in two dimensions as discrete spots and filaments (defined as linear-shaped signals which in fact may be more complex than a single filament) at the plasma membrane in both *S. pombe* and *A. gossypii* cells (Fig. 1*B*, Fig. S3, and Movie S1, S2). These signals could be seen moving all over the cell cortex and presumably have not been detected in previous studies due to the substantial cytosolic background fluorescence that obscures them in widefield or spinning disk confocal imaging.

To determine the composition of the signals, we calculated the number of fluorescent septin-mEGFP molecules in individual spots in *S. pombe* cells. To do this,

signal intensities of septins were detected and measured using custom MATLAB-based software. To estimate the number of fluorescent molecules in each spot, the measured intensity values of septin signals were compared to the intensity of mEGFP fused to a PH domain, previously shown to localize to plasma membrane in spots containing 1-2 molecules of mEGFP (Fig. 1*C*) (27).. Based on this calibration, septin spots contained highly variable numbers of fluorescent molecules with the vast majority greater in intensity than a predicted octameric complex, which we predict should be twice the intensity of a single mEGFP (population mean PH_{Num1}-mEGFP=1974 ± 820 a.u., N=1510 particles; Spn1-mEGFP=7,196 +/- 4,896 a.u., N=1774 particles; Fig. 1*C*). Thus, septins are found in complexes of heterogeneous size on the cortex of fission yeast cells

Fluorescent septin spots and short filaments collide and fuse, a process which we term “annealing”, and a number of these events occurring sequentially leads to the eventual formation of elongated filaments (Fig. 1*D*, Movie S1, S2 Fig. S3). Once formed, filaments can be observed to fragment (Movies S1 and S2). As the cell cycle progressed in *S. pombe*, short filaments localized to the center of the cell, annealed there and subsequently formed continuous bright ring structures at the site of cell division (Fig. 1*E* and Movie S3). Our results suggest that septins arrive at the plasma membrane from the cytosol as rod complexes, which then elongate through diffusion-mediated collisions and annealing to construct large assemblies.

Reconstitution of septin filament elongation

To determine if elongation by annealing is a fundamental behavior of septin complexes, or is mediated by other factors in the cell, we reconstituted septin assembly using recombinant proteins on supported lipid bilayers (Fig. S4*A*). *S. cerevisiae* septin complexes containing Cdc11-mEGFP, Cdc12-(His_6), Cdc3 and Cdc10 were co-expressed in *E. coli* and purified (Fig. S4*B*). Complexes were diluted to a final concentration of 0.5-3 nM of the octameric complex in low salt buffer (50 mM NaCl). We first determined the soluble state of purified septin complexes in a low-salt solution. Using FCS, we found septin-containing particles fluoresced to a median molecular brightness of slightly less than twice the value of purified mEGFP-(His_6). This intensity of signal is consistent with the interpretation that the majority of the population of septins are in complexes with two labeled septins (Fig. 2*A*). Purified septin complexes diffused at a mean of 31 ± 5 $\mu m^2/s$ in solution compared to 101 ± 6 $\mu m^2/s$ for purified mEGFP-(His_6) (Fig. 2*B*). This measured diffusion constant for septin complexes is consistent with a theoretical estimate for a rod with a diameter of 4 nm, a length of 32 nm and molecular weight of eight septin proteins (Fig. 2*C*). Thus, purified septins at low concentration (3 nM) in low salt solution likely exist as an octameric rod rather than elongated filaments.

We next added purified septin complex to supported lipid bilayers in an attempt to observe septin filament formation (Fig. 2*D* and Movie S5). Bilayers were prepared with 75:22:3 mol% phosphatidylcholine, phosphatidylinositol, phosphatidylinositol-4,5-bisphosphate and were judged to be fluid based on observation of two-dimensional diffusion of individual dye molecules when a trace amount of rhodamine-labeled phosphatidylethanolamine was included in the mixture (D= 1.46 ± 1.05 $\mu m^2/s$, N=25

particles; Fig. S4*C*, Movie S4). Septins were then monitored using TIRF microscopy to determine their behavior in the plane of the model lipid bilayer.

At 3 nM septin octamer, short filaments formed on the bilayer within 30 seconds enabling an analysis of the filament assembly process in real time (Fig. 2*D* and Movie S5). In order to determine the smallest unit of assembly, we measured the number of septin-GFP molecules in each diffraction-limited spot at the first moments of detection. To do this, we used custom MATLAB-based software to detect the spots and calibrated the measured intensities using intensity measurements of single molecules of pure mEGFP. Septin spots were initially found to fluoresce at an intensity comparable to ~2x mEGFP, supporting the conclusion that the rod complex containing two copies of Cdc11-mEGFP is the initial unit of assembly (Fig. 2E). Thereafter, fluorescent spots were continually recruited to the bilayer and an increase in the fluorescence intensity of each spot was noted with time (Fig. 2*F*). When combined, these data suggest Cdc11 is present in an octamer when it arrives at the membrane (with 2 molecules of Cdc11) and then rapidly forms short filaments (composed of multiple octamers) in the initial steps of assembly.

We then asked how filament formation was influenced by the concentration of septins in solution added to the bilayer. At 3 nM, puncta were clearly elongated in shape after 5-10 sec and within 30 sec, filaments of 1.5-2 μm were readily detected (Fig. 2G). Late in the assembly process at 3 nM, the network of septin filaments became too dense to accurately measure individual filament lengths; however, continued recruitment of septins to the bilayer was indicated by increasing fluorescence intensity (Fig. S4*D*). In contrast, at 1 nM, elongation occurred much slower and was found to

reach equilibrium at shorter filament lengths (Fig. 2G). The number of particles at the bilayer was found to increase from the initial addition of septins through elongation and this count represents a balance between recruitment of new particles from solution and merging of particles into filaments over time (Fig. 2H). Notably, elongated puncta and very short filaments could be seen at concentrations as low as 0.5 nM. These data support that the length of filaments and kinetics of assembly are impacted by the concentration of septins used in the assay.

Septins elongate by annealing on supported lipid bilayers

We next examined the mechanism of filament elongation on supported lipid bilayers. Filaments were defined as elongated structures that moved as a single unit. The elongated structures were produced by fusion of rod complexes to produce short filaments and subsequently short filaments merged together to form longer filaments (Fig. 3*A* and Movie S6). Thus, pure septin complexes on diffusive lipid bilayers recapitulated the annealing behavior observed in vivo.

We then evaluated if filament length impacts annealing events or diffusive behavior of complexes on the membrane. We wondered if there was any bias in the size of filaments that anneal however we could not detect a systematic pattern in the sizes of filaments that participate in an annealing event (Fig. 3*B, C*). This means that filaments can merge regardless of their relative sizes. This property can be seen when we calculate the difference in length between two filaments that anneal and compare this measured distribution to a distribution made from a simulation in which the same collection of filaments are paired at random (Fig. 3*C,* no significant difference between

observed and simulated random distribution). Length does, however, have a modest impact on filament diffusion rates in that we detect a moderate negative correlation between filament length and diffusion rate as measured by mean square displacement (r=-0.42, mean 0.16 $\mu m^2/s$, Fig. 3*D*). Thus, filament length does not restrict septin annealing events directly however filament length does modestly impact rates of diffusion.

Next, we evaluated whether filaments can elongate at both free ends and if subunits can be incorporated in the middle/sides of a pre-existing filament. For these experiments, septin complexes containing Cdc11-mCherry were purified and mixed with Cdc11-mEGFP complexes. Specifically, Cdc11-mEGFP complexes were first assembled on a supported lipid bilayer and excess, non-membrane bound complexes were removed. Cdc11-mCherry septin complexes were then added and the locations of new addition were monitored. We found addition occurred at filament ends and in many cases pre-formed filaments elongated at both ends (Fig. 4*A,* Movie S7). The majority of newly incorporated septin arrived at preformed filament ends after 2D diffusion on the membrane rather than arriving directly from the bulk solution (81%, N=21). No Cdc11mCherry-labeled complexes were found to add to the middle of pre-existing green filaments. Over time, however, mCherry subunits could be seen in the middle of filaments due to repeated fragmentation and re-annealing of the original GFP-labeled filaments. These results support the conclusion that elongation occurs exclusively at the ends of pre-existing filaments and suggest that septins do not exchange subunits internally or bind to sides of pre-existing filaments in these conditions.

In addition to annealing, fragmentation of filaments was also readily observed in vitro as in vivo (Fig. 4*B* and Movie S8). Filaments can fragment at a variety of places and breakage is not limited to the ends or the middle. Fragmentation occurred after filaments would bend indicating that the flexibility is integral to setting the filament length and stability on the bilayer.

To measure the flexibility of septin filaments, bending over time was used to determine persistence length. Persistence length is a measure of the stiffness of a polymer, and we calculated this property of septins as described by Gittes *et al.* for actin and microtubules (28). Septins were found to have a median persistence length of 12 μm on bilayers and there was no correlation between filament length and persistence length (Fig. 4*C*). These estimates are in contrast to 18 μm for actin and 5,200 μm for microtubules on glass. These measurements support that septins are highly flexible filaments and that in this reconstituted setting these are unlikely to be bundled filaments.

In vitro, two possible mechanisms could favor septin filament elongation on supported lipid bilayers rather than in solution. It is possible that an effective concentration increase and restriction of diffusion to two dimensions controls the formation of septin filaments. Alternatively, a phosphatidylinositol-induced conformational change that occurs within septins upon association with the membrane could promote filament formation. To differentiate between these two scenarios, an alternative approach to bilayer recruitment was utilized. Because septin complexes were purified using Cdc12-(His_6), bilayers containing 4% DGS-NTA(Ni) lipids and 96% phosphatidyl choline were prepared and analyzed for their ability to promote septin filament assembly (Fig. 4D). The same property of elongation by annealing was

observed on membranes of this composition of lipids although the assembly of filaments was slower than in phosphatidylinositol-containing bilayers (Movie S9). Notably, no filaments formed when purified septin complexes were added to cleaned, casein- or BSA-coated glass indicating that diffusion provided by a fluid membrane is a critical component of filament assembly at low septin concentrations (Fig. S4*E*). Thus, in a reduced system containing septin heteromeric complexes and a supported lipid bilayer, septins assemble filaments and higher-order structures through two-dimensional diffusion and annealing. These data suggest that annealing is a fundamental property of the septin polymer that drives the assembly process.

Discussion

Dynamic transitions between soluble and assembled states lend cytoskeletal polymers many of their functional properties, from force generation and motility to contraction and scaffolding (29, 30). Based on the work reported here, we are able to propose a three-step process for the formation of septin assemblies (Fig. 4*E*). First, as measured by FCS, septins oligomerize into small complexes that are not filaments in the cytoplasm. These complexes are likely to be rods that are heterooctamers or decamers in fungi based on previous work with purified and recombinant proteins in high salt conditions (17, 18, 31, 32). Subsequently, when rods contact the plasma membrane, they are concentrated, diffuse and merge to grow into short filaments through annealing. These short filaments then diffuse in the plane of the membrane merging into each other and nascent higher-order structures such as the rings and collars that demarcate sites of cytokinesis in fungal cells (Fig. 4*E*). In summary, this

study shows septin membrane associations effectively concentrate subunits and limit the dimensionality of diffusion to promote filament formation.

In cells, it is unknown what controls the ratio of the amount of septins on the plasma membrane to the amount in the cytoplasm. It is interesting to note that septins assemble in vitro at concentrations that are orders of magnitude lower than the measured cytoplasmic concentration of septins. This could indicate that even at high concentrations, 3-dimensional diffusion is insufficient to support annealing of rods in the cytosol. Alternatively there could be a conformational change induced by membrane association or a capping protein that dissociates at the membrane to restrict the location of elongation. This possible function of the membrane need not necessarily be phosphoinositide-dependent based on the in vitro experiments where filaments form with Ni-NTA-based recruitment (Fig. 4). It will be critical in the future to determine if septin rods are capped to limit cytosolic polymerization and if the membrane provides a distinct role in assembly beyond restricting diffusion to two dimensions.

With the reconstitution assay, we can make predictions as to the mechanisms driving septin polymerization. We speculate filaments form through what is likely an isodesmic rather than cooperative, nucleation-elongation process. An isodesmic assembly is consistent with a relatively low concentration for polymerization in the presence of a membrane and a broad filament size distribution (33). It is possible that in early stages of assembly, in diffraction-limited spots, septins do cooperatively assemble via a process not detectable by this assay. Furthermore, it is possible that the assembly of heteromeric rods in the cytosol is a cooperative process that cannot be monitored using present approaches in vivo. Mixed (ie isodesmic and cooperative) modes of

assembly have been speculated to exist for FtsZ and even actin, displays isodesmic or nucleation-elongation assembly kinetics depending on the species of origin (33). For example, animal F-actin assembly clearly displays a nucleation-elongation mechanism of assembly, while parasite F-actin forms by an isodesmic process reminiscent of what we see with septins on membranes (35).

The behavior of septins in the vitro assay supports the conclusion that filament assembly begins with the recruitment of individual septin rods from solution to membranes and that filament growth progresses in a bidirectional, end-dependent manner. It is clear new rods are not added in the middle of pre-made filaments; nor do they associate with the sides of pre-existing filaments. This indicates both that exchange of subunits within a filament does not occur under these conditions and that rods are not joining filaments by lateral associations but rather by only end-on associations. Furthermore, in vitro, we do not see filaments elongate due to addition of subunits arriving from the bulk solution but rather primarily through collisions between particles diffusing in two dimensions. Importantly, in vivo it cannot be determined if soluble septins are also able to join larger assemblies directly from the cytosol in addition to diffusion-driven annealing. Analyzing this process in vivo is complicated by the fact that it is unclear if all septin filaments are membrane associated or if there are layers of septin filaments stacked on membranes with some filaments directly binding membranes and some filaments associating with other filaments. Future work in vivo should consider how to address the issue of exchange of subunits within filaments and bundling in assembled higher-order structures. These facets of septin assembly likely

require additional cytosolic factors, post-translational modifications and/or lateral associations between filaments.

How do the properties of septins we have found here in terms of flexibility, annealing and fragmentation relate to the properties of higher-order structures of septins in cells? We speculate that flexibility of filaments and their capacity to anneal may accelerate assembly, rearrangement and disassembly of higher-order structures. Previous work using polarization microscopy has demonstrated that the septin hour-glass structure in yeast is anisotropic suggesting it is highly ordered both before and after cytokinesis (13, 36, 37). We imagine that the order emerges from a septin binding or bundling partner that constrains and contains the flexible filaments. Alternatively, tight lateral associations between adjacent filaments may be sufficient to bundle filaments and create the highly anisotropic assemblies observed in cells. If present, these lateral associations either form in a concentration-dependent manner or require a cytosolic factor because we did not obtain any evidence for lateral associations on membranes in vitro. Despite appearing highly anisotropic through most of the cell cycle, the septin hourglass displays a notably more “fluid” or isotropic transition at cytokinesis (1, 13, 36, 37). The flexibility, annealing and fragmentation properties are likely important for transit through the isotropic phase. The loss, addition or modification of a binding partner or septins themselves could initiate this transition seen by polarization microscopy at cytokinesis. Future work adding in putative septin regulators to the in vitro system will be illuminating to determine if any cell-cycle regulated, septin-binding proteins can bring order to flexible filaments.

This report represents the first reconstitution of septin polymerization in vitro that captures and quantitatively measures the dynamics of septin assembly on a bilayer. This will be a powerful model system on which to test the role of nucleotides, post-translational modifications and accessory factors on the organization of septins. By combining a reconstitution assay with live cell imaging, this work reveals a role for a plasma membrane in driving septin filament elongation and the construction of higher-order assemblies.

Materials and Methods

Supported Lipid Bilayer Preparation

Supported lipid bilayers were prepared on clean glass as detailed in supporting information. Briefly, after sonication and plamsma cleaning, small unilamellar vesicles (SUVs) of desired lipid mixture were prepared by rehydration and bath sonication until the solution clarified and SUVs were allowed to fuse with glass. Bilayers were washed with 50 mM Tris pH 8.0, 300mM NaCl, 1 mg/mL fatty acid free bovine serum albumin (Sigma A6003) before the addition of septins. Detailed methods can be found in the supporting information.

Image Analysis

Images were processed and analyzed using ImageJ, MATLAB, and Nikon Elements software (38). Detailed descriptions of particle detection, tracking, and quantification can be found in the supporting information.

Acknowledgements

We would like to thank the labs of T. Mitchison, C. Field, R. Oldenbourg, and the cytoskeletal community at Dartmouth for thoughtful discussion; R. Sloboda for critically reading the manuscript, M. Loose for training in the preparation of supported lipid bilayers; A. Lavanway for support with microscopes; JQ Wu, J. Moseley, and H. Ewers for sharing strains; C. Anderson for statistical advice; J. Mayor and D. Köster for lipids and protocols; and J. Thorner for sharing plasmids. This project was supported with funding from by NSF (MCB-507511, ASG) and NIH (GM100160, TT and ASG), and Colwin, Lemann and Spiegel summer fellowships and The Nikon Award for summer investigation at MBL in Woods Hole, MA (ASG) and instrument support from Micro Video Instruments (MVI).

References

1. Dobbelaere J & Barral Y (2004) Spatial coordination of cytokinetic events by compartmentalization of the cell cortex. *Science* 305(5682):393-396.
2. Gilden JK, Peck S, Chen YC, & Krummel MF (2012) The septin cytoskeleton facilitates membrane retraction during motility and blebbing. *The Journal of cell biology* 196(1):103-114.
3. Byers B & Goetsch L (1976) A highly ordered ring of membrane-associated filaments in budding yeast. *The Journal of cell biology* 69(3):717-721.
4. Oh Y & Bi E (2011) Septin structure and function in yeast and beyond. *Trends in cell biology* 21(3):141-148.
5. Culotti J & Hartwell LH (1971) Genetic control of the cell division cycle in yeast. 3. Seven genes controlling nuclear division. *Experimental cell research* 67(2):389-401.
6. Kinoshita A*, et al.* (1998) Identification of septins in neurofibrillary tangles in Alzheimer's disease. *The American journal of pathology* 153(5):1551-1560.
7. Hall PA & Russell SE (2004) The pathobiology of the septin gene family. *The Journal of pathology* 204(4):489-505.
8. Russell SE & Hall PA (2011) Septin genomics: a road less travelled. *Biological chemistry* 392(8-9):763-767.
9. Dagdas YF*, et al.* (2012) Septin-mediated plant cell invasion by the rice blast fungus, Magnaporthe oryzae. *Science* 336(6088):1590-1595.
10. Mostowy S*, et al.* (2010) Entrapment of intracytosolic bacteria by septin cage-like structures. *Cell host & microbe* 8(5):433-444.
11. Ryder LS*, et al.* (2013) NADPH oxidases regulate septin-mediated cytoskeletal remodeling during plant infection by the rice blast fungus. *Proceedings of the National Academy of Sciences of the United States of America* 110(8):3179-3184.
12. Tooley AJ*, et al.* (2009) Amoeboid T lymphocytes require the septin cytoskeleton for cortical integrity and persistent motility. *Nature cell biology* 11(1):17-26.
13. DeMay BS*, et al.* (2011) Septin filaments exhibit a dynamic, paired organization that is conserved from yeast to mammals. *The Journal of cell biology* 193(6):1065-1081.
14. Gladfelter AS, Bose I, Zyla TR, Bardes ES, & Lew DJ (2002) Septin ring assembly involves cycles of GTP loading and hydrolysis by Cdc42p. *The Journal of cell biology* 156(2):315-326.
15. Beise N & Trimble W (2011) Septins at a glance. *Journal of cell science* 124(Pt 24):4141-4146.
16. Spiliotis ET & Gladfelter AS (2012) Spatial guidance of cell asymmetry: septin GTPases show the way. *Traffic* 13(2):195-203.
17. Bertin A*, et al.* (2008) Saccharomyces cerevisiae septins: supramolecular organization of heterooligomers and the mechanism of filament assembly. *Proceedings of the National Academy of Sciences of the United States of America* 105(24):8274-8279.

18. Frazier JA*, et al.* (1998) Polymerization of purified yeast septins: evidence that organized filament arrays may not be required for septin function. *The Journal of cell biology* 143(3):737-749.
19. Barral Y & Kinoshita M (2008) Structural insights shed light onto septin assemblies and function. *Current opinion in cell biology* 20(1):12-18.
20. John CM*, et al.* (2007) The Caenorhabditis elegans septin complex is nonpolar. *The EMBO journal* 26(14):3296-3307.
21. Sirajuddin M*, et al.* (2007) Structural insight into filament formation by mammalian septins. *Nature* 449(7160):311-315.
22. Bertin A*, et al.* (2010) Phosphatidylinositol-4,5-bisphosphate promotes budding yeast septin filament assembly and organization. *Journal of molecular biology* 404(4):711-731.
23. Zhang J*, et al.* (1999) Phosphatidylinositol polyphosphate binding to the mammalian septin H5 is modulated by GTP. *Current biology : CB* 9(24):1458-1467.
24. Casamayor A & Snyder M (2003) Molecular dissection of a yeast septin: distinct domains are required for septin interaction, localization, and function. *Molecular and cellular biology* 23(8):2762-2777.
25. Murphy DB, Gray RO, Grasser WA, & Pollard TD (1988) Direct demonstration of actin filament annealing in vitro. *The Journal of cell biology* 106(6):1947-1954.
26. Wu JQ & Pollard TD (2005) Counting cytokinesis proteins globally and locally in fission yeast. *Science* 310(5746):310-314.
27. Tang X, Punch JJ, & Lee W (2009) A CAAX motif can compensate for the PH domain of Num1 for cortical dynein attachment. *Cell Cycle* 8(19):3182-3190.
28. Gittes F, Mickey B, Nettleton J, & Howard J (1993) Flexural rigidity of microtubules and actin filaments measured from thermal fluctuations in shape. *The Journal of cell biology* 120(4):923-934.
29. Mitchison T & Kirschner M (1984) Dynamic instability of microtubule growth. *Nature* 312(5991):237-242.
30. Estensen RD*, et al.* (1971) Cytochalasin B: microfilaments and "contractile" processes. *Science* 173(3994):356-359.
31. Field CM*, et al.* (1996) A purified Drosophila septin complex forms filaments and exhibits GTPase activity. *The Journal of cell biology* 133(3):605-616.
32. Meseroll RA, Howard L, & Gladfelter AS (2012) Septin ring size scaling and dynamics require the coiled-coil region of Shs1p. *Molecular biology of the cell* 23(17):3391-3406.
33. Romberg L, Simon M, & Erickson HP (2001) Polymerization of Ftsz, a bacterial homolog of tubulin. is assembly cooperative? *The Journal of biological chemistry* 276(15):11743-11753.
34. Chen Y, Bjornson K, Redick SD, & Erickson HP (2005) A rapid fluorescence assay for FtsZ assembly indicates cooperative assembly with a dimer nucleus. *Biophysical journal* 88(1):505-514.
35. Skillman KM*, et al.* (2013) The unusual dynamics of parasite actin result from isodesmic polymerization. *Nature communications* 4:2285.
36. Vrabioiu AM & Mitchison TJ (2006) Structural insights into yeast septin organization from polarized fluorescence microscopy. *Nature* 443(7110):466-469.

37. DeMay BS, Noda N, Gladfelter AS, & Oldenbourg R (2011) Rapid and quantitative imaging of excitation polarized fluorescence reveals ordered septin dynamics in live yeast. *Biophysical journal* 101(4):985-994.
38. Schneider CA, Rasband WS, & Eliceiri KW (2012) NIH Image to ImageJ: 25 years of image analysis. *Nature methods* 9(7):671-675.

Figure Legends

Fig. 1: Septins grow by annealing on the plasma membrane of *S. pombe*. (A) Molecular brightness and diffusion coefficient of cytoplasmic Spn1-mEGFP (AGY093) determined by FCS compared to cells expressing cytoplasmic mEGFP (AGY109) alone in *S. pombe*. Box plots display median, lower and upper quartiles and whiskers show range N>20 cells, ***P<0.001 by Kruskal Wallace one way analysis of variance. (B) Spn1-mEGFP particles and short filaments localized on the cortex of *S. pombe* monitored using TIRF microscopy. Heat maps represent relative particle intensities. Arrows on the intensity scale indicate the estimated intensity of a complex containing two Cdc11-mEGFP molecules, ~4000 a.u., based on calibration. Cell outlines are shown in white. (C) Distribution of PH_{Num1}-GFP and Spn1-mEGFP particle intensities on the plasma membrane measured from images collected using the same laser intensity and exposure time. (D) Annealing event between two diffusing short septin filaments on the cell cortex of *S. pombe*. Arrows indicate particles involved in annealing. Cell outines are shown in white. (E) Formation of Spn1-mEGFP septin ring by annealing of intermediate size particles at the plane of division in *S. pombe*. Cell outines are shown in white. With the exception of FCS (Panel A), all images were acquired using TIRF microscopy.

Fig. 2: Reconstituted septin assembly on supported lipid bilayers. (A) Molecular brightness of pure mEGFP compared to co-purified, recombinant septins containing Cdc11-mEGFP in solution, as measured by FCS. Box plots display median, lower and upper quartiles and whiskers show range. ***P<0.001 by Kruskal Wallace one way analysis of variance. (B) Diffusion coefficients of pure mEGFP compared to Cdc11-

mEGFP containing septin complexes, estimated by fitting FCS results to a single component anamolous diffusion model. (C) Diffusion coefficients were predicted for complexes of different numbers of septin octamers using previously measured dimensions (i.e. length = 32 nm; diameter = 4 nm; MW = 443 kDa) modeled as either a rod-like or spherical in organization for a given molecular weight. Horizontal black line is measured diffusion constant, red asterisks are predicted diffusion constants for septin complexes in a rod-like shape, blue asterisks are diffusion constants of complexes arranged in a sphere. (D) Cdc11-mEGFP signal accumulates and forms filaments at the lipid bilayer over time (3 nM octamer concentration) monitored by TIRF microscopy. (E) Quantification of fluorescence intensity (background subtracted) of single molecules of mEGFP (green histogram) and Cdc11-mEGFP complexes in the first moment of arrival at the bilayer (3 nM, blue histograms). (F) TIRF microscopy was used to measure septin particle brightness in each frame during the first 8 seconds of assembly (3 nM) in conditions where single molecules of mEGFP fluoresce to 100 a.u. The number of particles of a given intensity is represented by the color code beside the plot. (N>10,000 particles (G) Filament length was measured over time and the mean length of elongated particles is plotted for each timepoint in a 3 nM and 1 nM mixture of septin complex. (H) Particle count and filament length over time in 1 nM assembly (same data as (G)). Values were normalized to maximum values of length or particle count and minimum values were set to zero. These values were fit and plotted normalized to the curve.

Fig. 3: Septin filaments grow by annealing on supported lipid bilayers. (A) Representative TIRF image series of filament growth by annealing. Arrows indicate short filaments that merge. (B) Measured filament lengths prior to annealing and after

annealing are plotted (N=40 annealing events). (C) The length difference between pairs of filaments prior to annealing is shown in the histogram. These filaments that participated in annealing events were then paired at random, differences were calculated from the random pairs and plotted as red line. The simulated random distribution of differences is not distinguishable from the actual data (insignificant two-sample Kolmogorov-Smirnov test). (D) Filament length and diffusion coefficients were measured and plotted for a population of septin particles at the bilayer.

Fig. 4: Septin filaments elongate at ends, are flexible, and can be formed on a membrane without phosphatidylinositide. (A) Cdc11-mEGFP septin filaments were assembled on bilayer, unbound complexes were washed out and Cdc11-mCherry complexes were added and monitored in TIRF. Addition of new complexes occurred at both filament ends. (B) Cdc11-mEGFP filaments fragment on a supported lipid bilayer. Arrows indicate site of fragmentation event and new short filaments arising from the break. (C) Example of filament bending image series used for determining persistence length of septin filaments. Arrow indicates bending filament. Box plot shows a median persistence length of 12 µm. Filaments used ranged between 1.2-2.1 µm, with a median of 1.8 µm (N=10). Box plots display median, lower and upper quartiles and whiskers show range. (D) Cdc11-mEGFP containing septin filaments assembled on supported lipid bilayers containg 96% phosphatidylcholine and 4% DGS-NTA(Ni). (E) Model. 1) Septins arrive at plasma membranes from cytoplasm as short rods. 2) Rods then assemble into short filaments on the plasma membrane through annealing. 3) Short filaments then build higher order structures.

Figure 1

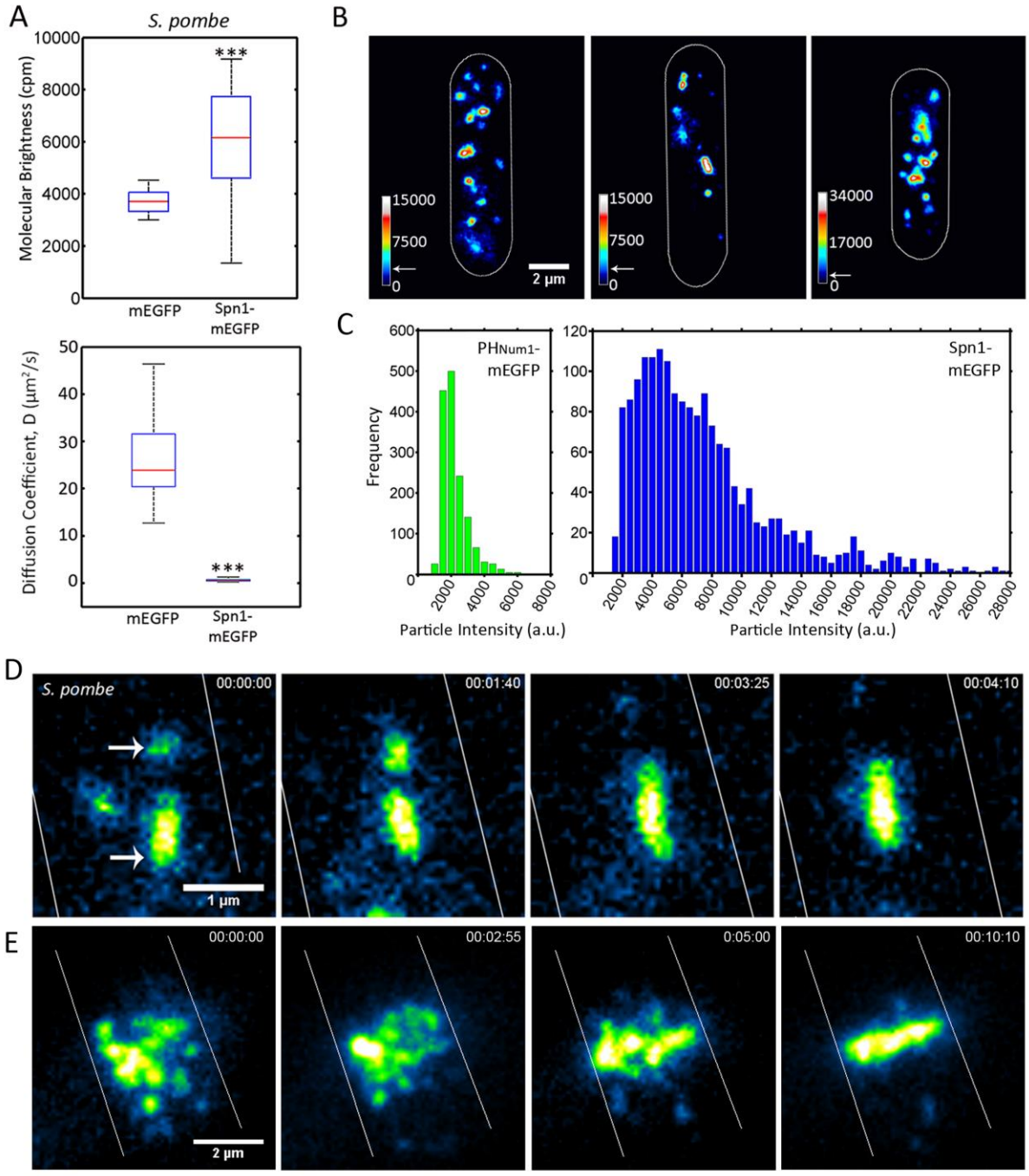
A
S. pombe
Molecular Brightness (cpm)
10000
8000
6000
4000
2000
0
***
mEGFP
Spn1-mEGFP
Diffusion Coefficient, D (μm²/s)
50
40
30
20
10
0
***
mEGFP
Spn1-mEGFP
B
15000
7500
0
2 μm
15000
7500
0
34000
17000
0
C
Frequency
PHNum1-mEGFP
Particle Intensity (a.u.)
Spn1-mEGFP
Particle Intensity (a.u.)
D
S. pombe
00:00:00
00:01:40
00:03:25
00:04:10
1 μm
E
00:00:00
00:02:55
0:05:00
00:10:10
2 μm

Figure 2

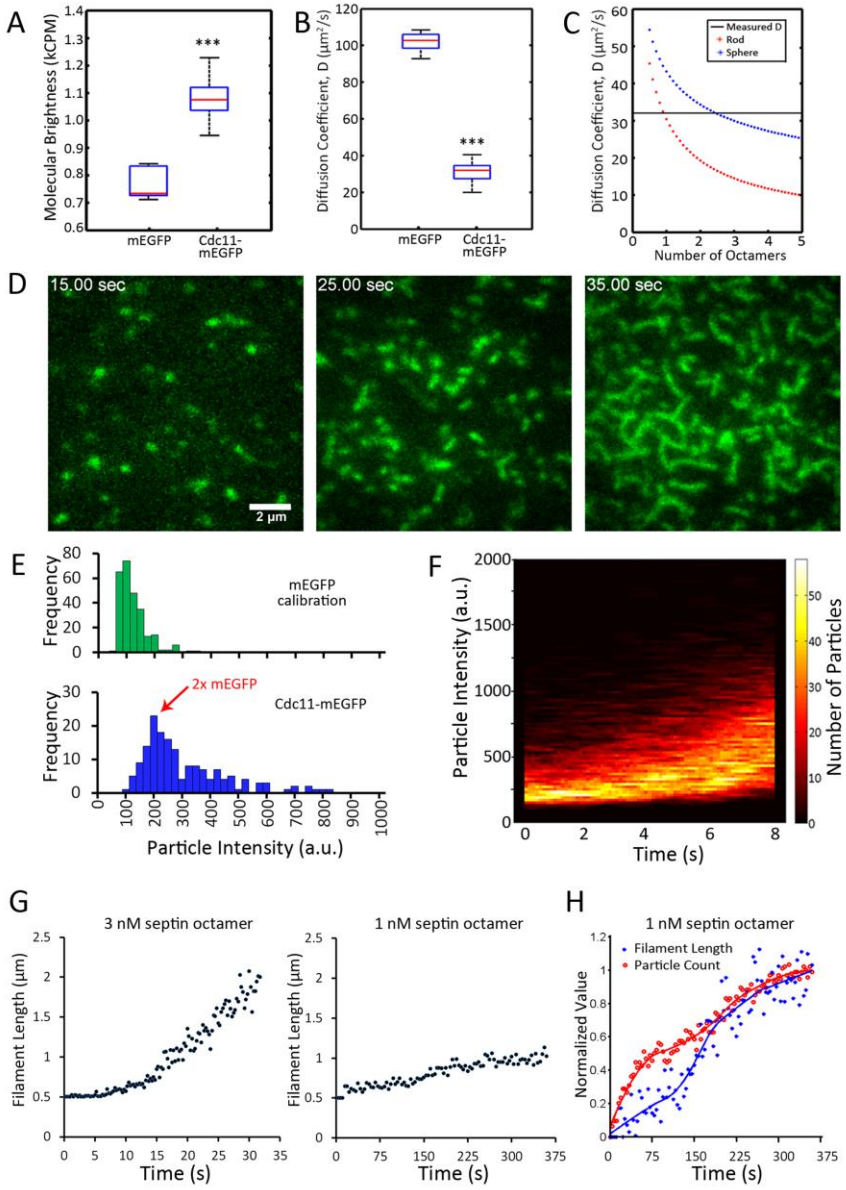
A
Molecular Brightness (kCPM)
***
mEGFP
Cdc11-mEGFP
B
Diffusion Coefficient, D (μm²/s)
***
mEGFP
Cdc11-mEGFP
C
Diffusion Coefficient, D (μm²/s)
Measured D
Rod
Sphere
Number of Octamers
D
15.00 sec
25.00 sec
35.00 sec
2 μm
E
Frequency
mEGFP calibration
2x mEGFP
Cdc11-mEGFP
Particle Intensity (a.u.)
F
Particle Intensity (a.u.)
Number of Particles
Time (s)
G
3 nM septin octamer
1 nM septin octamer
Filament Length (μm)
Time (s)
H
1 nM septin octamer
Filament Length
Particle Count
Normalized Value
Time (s)

Figure 3

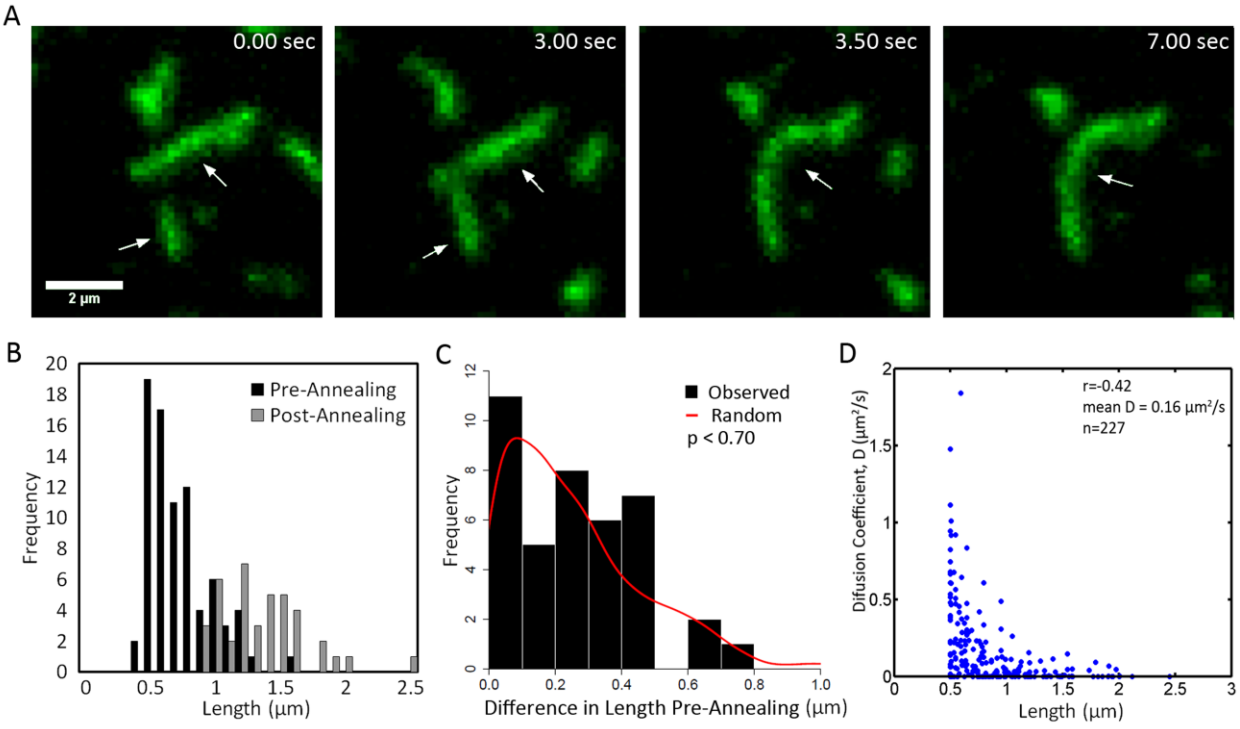
A
0.00 sec
3.00 sec
3.50 sec
7.00 sec
2 µm
B
Pre-Annealing
Post-Annealing
Frequency
Length (µm)
C
Observed
Random
p < 0.70
Frequency
Difference in Length Pre-Annealing (µm)
D
r=-0.42
mean D = 0.16 µm²/s
n=227
Difusion Coefficient, D (µm²/s)
Length (µm)

Figure 4

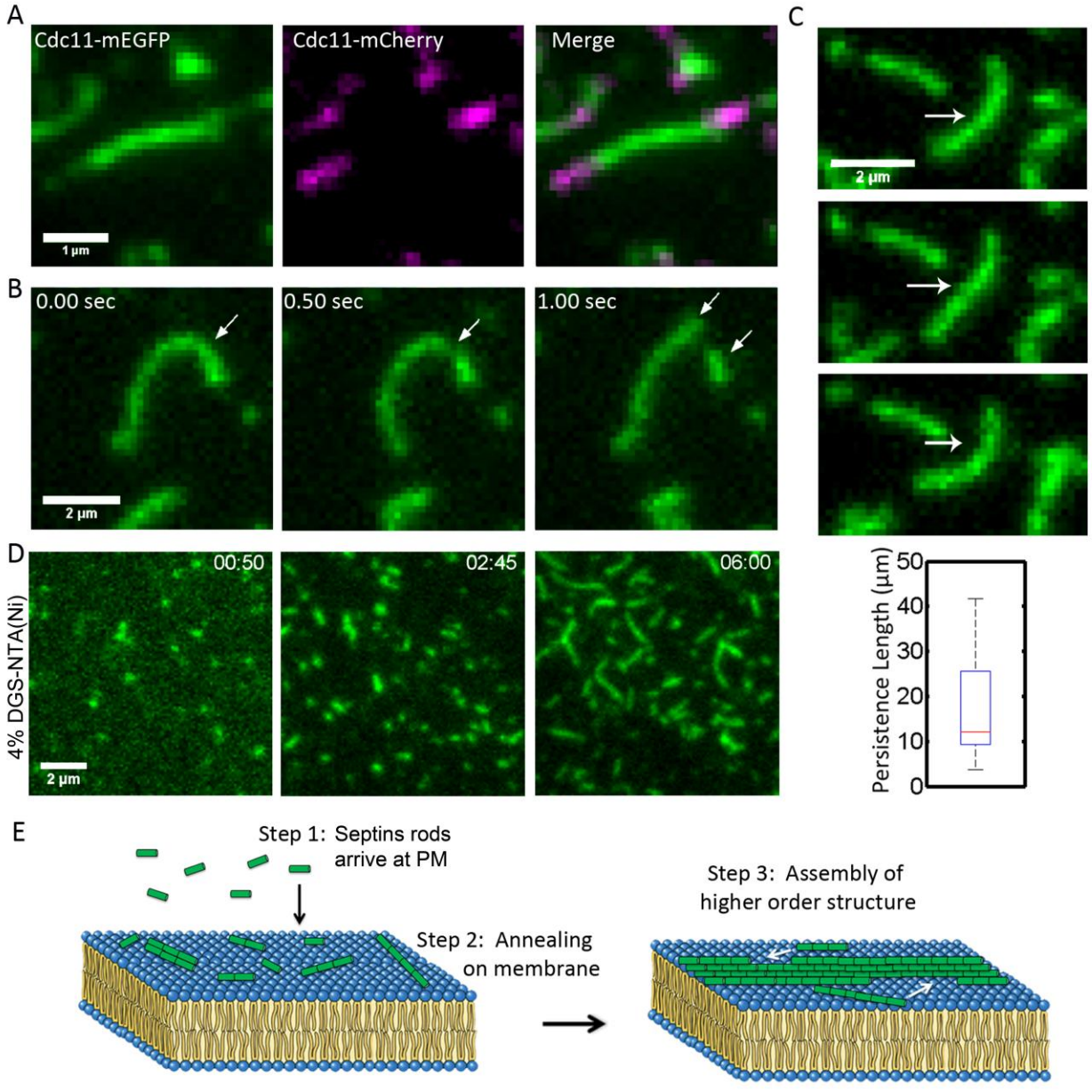
A
Cdc11-mEGFP
Cdc11-mCherry
Merge
1 µm
B
0.00 sec
0.50 sec
1.00 sec
2 µm
C
2 µm
D
4% DGS-NTA(Ni)
00:50
02:45
06:00
2 µm
Persistence Length (µm)
50
40
30
20
10
0
E
Step 1: Septins rods arrive at PM
Step 2: Annealing on membrane
Step 3: Assembly of higher order structure

Supporting Information

SI Materials and Methods

Construction of pMVB133-*Sc*Cdc11-mEGFP and pMVB133-ScCdc11-mCherry

pMVB133 pACYC-Duet with *Sc*Cdc3 and *Sc*Cdc11 and pMVB128 pET-Duet with His6*Sc*Cdc12 and *Sc*Cdc10 were gifts from the lab of Jeremy Thorner. To tag Cdc11 with mEGFP, a SpeI site was engineered into pMVB133 (AGB400.1) using AGO 1170 (MVB133 SpeI F) and AGO1171 (MVB133 SpeI R) to generate AGB452 (MVB133 SpeI) using the QuikChange XL kit from Agilent Technologies. Point mutations were verified by sequencing through the region with AGO1088 (*Sc*Cdc11 IV) and AGO1176 (MVB133 *Sc*Cdc11 DS R). A PCR template was used to amplify GFP by digesting AGB010 (pAGT101, GFP::NAT) with BglI. The template was cleaned by gel extraction with Qiagen Gel Extraction Kit and PCR was performed with AGO1174 (*Sc*Cdc11-GFP SpeI F) and AGO1175 (*Sc*Cdc11-GFP SpeI R) to obtain a 1009bp product with SpeI sites on both ends. The SpeI-GFP PCR product and AGB452 were digested with SpeI and the ligated product was verified with EcoRV/NdeI. The plasmid was sequenced with AGO208, 405, 1088, 1176. After sequencing, the plasmid was transformed into BL21 (DE3) competent cells for expression along with pMVB128 (AGB401.1).

To produce pMVB133-ScCdc11-mCherry, AGB483 (pRS416-ScCdc11-mCherry) and AGB400.2 (pMVB133) were cut with EcoRI-HF/KpnI-HF. The vector was treated with CIP (Roche DiagnosticsGmbH, Mannheim, Germany) and ligation was performed using NEB T4 ligase. The plasmid was verified by digestion with AflII/AleI and was transformed into BL21 (DE3) competent cells for expression along with AGB401.1.

Oligos were synthesized by Integrated DNA Technologies, Inc., Coralville, Iowa. Restriction enzymes and competent cells were purchased from New England Biolabs Inc., Ipswich MA. Sequencing was performed at the Molecular Biology and Proteomics Core Facility, Dartmouth College, Hanover, NH.

Protein Expression and Purification

BL21 (DE3) *E. coli* cells were transformed with the duet septin expression platform, selected for with ampicillin and chloramphenicol, and induced to express with 1mM IPTG at an OD600 of 0.6-0.7. After 24 hours of growth at 22^{o}C, cells were harvested by centrifugation at 10,000 RCF for 15 minutes. Pellets were stored at -80^{o} C until lysis. Cells were thawed and incubated in lysis buffer (50 mM NaH_2PO_4 pH 8.0, 1M NaCl, 1 mM $MgCl_2$, 1% Tween-20, 10% Glycerol, 1X Protease Inhibitor (Roche), 40 mM Imidazole) with 1 mg/mL lysozyme for 30 minutes on ice. Cells were then sonicated and resulting whole cell extract was clarified by centrifugation at 4^{o}C for 30 minutes at 13,000 xg. Clarified supernate was placed on equilibrated NiNTA spin columns (Qiagen), washed three times with wash buffer (50 mM NaH_2PO_4 pH 8.0, 1M NaCl, 40 mM Imidazole), and eluted with a high imidazole concentration (50 mM NaH_2PO_4 pH 8.0, 300mM NaCl, 500 mM Imidazole). Protein was then dialyzed into septin storage buffer (50 mM Tris pH 8.0, 300 mM NaCl) overnight in two 500 mL steps using 10,000 dalton MW cutoff cassettes (Thermo Scientific). Purity was assessed by 10% SDS-PAGE and protein concentration was determined by Bradford assay.

Fungal Cell Culture

S. cerevisiae cells were grown in YPD media overnight at 30^{o}C to an OD600 0.2-0.5 and imaged on low fluorescent yeast media agar pads at 22^{o}C. *S. pombe* cells were

grown in YE4S media overnight at 30^{o}C to an OD600 0.2-0.5 and imaged on EMM4S media agar pads at 22^{o}C. *A. gossypii* cells were grown in AFM media overnight at 30^{o}C for 16 hours and imaged on low fluorescent minimal media agar pads at 22^{o}C.

Supported Lipid Bilayer Preparation

Glass coverslips were prepared by sequential 30 minute sonication steps in 3 N KOH, 100% ethanol, and ddH_2O with ddH_2O rinses between each. Coverslips were dried and exposed to plasma for 10 minutes. Small unilamellar vesicles (SUVs) of desired lipid mixture were prepared by removing chloroform solvent with a stream of nitrogen gas followed by at least 2 hours in a vacuum, rehydration in 20mM Tris pH 8.0, 300 mM KCl, 1mM $MgCl_2$, 1mM $CaCl_2$, and bath sonication until the solution clarified. Plastic chambers were glued to cleaned coverslips and SUVs were allowed to fuse with glass for 30 minutes at 37^{o} C. After fusion, bilayers were washed with 1 mL of buffer (20mM Tris pH 8.0, 300 mM KCl, 1mM $MgCl_2$). Immediately before addition of septins, bilayers were washed with 50 mM Tris pH 8.0, 300mM NaCl, 1 mg/mL fatty acid free bovine serum albumin (Sigma A6003). Bilayers were prepared with 75 mol% L-α-phosphatidylcholine (Egg, Chicken, Avanti Polar Lipids 840051), 22% L-α phosphatidylinositol (Liver, Bovine, sodium salt, Avanti Polar Lipids 840042), and 3% L-α-phosphatidylinositol-4,5-bisphosphate (Brain, Porcine, ammonium salt, Avanti Polar Lipids 840046). The integrity and diffusability of bilayers were periodically monitored by adding trace L-α-Phosphatidylethanolamine-N-(lissamine rhodamine B sulfonyl, Ammonium Salt, Egg-Transphosphatidylated, Chicken, Avanti Polar Lipids 810146).

To prepare bilayers containing 96 mol% L-α-phosphatidylcholine (Egg, Chicken, Avanti Polar Lipids 840051), and 4 mol% 1,2-di-(9Z-octadecenoyl)-*sn*-glycero-3-[(N-(5-

amino-1-carboxypentyl)iminodiacetic acid)succinyl] (nickel salt, Avanti Polar Lipids 790404), lipids were mixed in chloroform solvent, dried by a stream of nitrogen gas followed by at least 2 hours in a vacuum. Lipids were hydrated in 150 mM NaCl and 20 mM Hepes pH 8.0 and freeze-thawed on liquid nitrogen ten times. Vesicles were bath sonicated to clarity, and centrifuged at 4^{o}C at 13,000 xg for 45 minutes. Supernatant was placed in chambers on cleaned coverslips and washed with buffer as described above.

Total Internal Reflection Fluorescence Microscopy

Septins on supported lipid bilayers and in fungal cells were imaged using total internal reflection fluorescence microscopy to limit excitation to fluorophores proximal to the coverslip. A homemade optical setup with a fluorescence microscope, TE 2000-E: Nikon, 100x PlanApo TIRF, NA 1.49: Nikon, was used to monitor Cdc11-mEGFP on supported bilayers. A laser light from a 20 mW, 488 nm diode pumped solid-state laser (Melles Griot, Carlsbad, CA, USA) was introduced into the microscope through an optical path installed on a vibration insulation table (Herz, Yokohama, Japan). Neutral density filters and an electro-magnetic shutter (Vincent associates, Rochester, NY, USA) were placed in the optical path. Excitation optics were composed of a dual-beam, TIRF-illumination system that ensured uniform excitation of fluorescent molecules. The excitation laser beam was split into two linearly polarized beams steered by tunable mirrors into the periphery of the back focal plane of the objective lens so that they crossed each other in the specimen space at right angle. Collected fluorescence was focused on an electron-multiplied CCD camera (iXon plus, Andor Technology, UK) In

Fig 4 (*A-C)*, to achieve high signal to noise ratios, excess septin complexes not bound to the bilayer were washed out and replaced with buffer.

Fungal cells were imaged using a commercially available TIRF microscope distributed by Micro Video Instruments (MVI) with a 60 mW, 488 nm laser through a Nikon Apo TIRF 100X oil 1.49NA and an Andor iXon Ultra EMCCD camera.

Image Analysis

Images were processed and analyzed using ImageJ, MATLAB, and Nikon Elements software (4). Prior to particle intensity measurements of TIRF images, uniform background subtractions were performed. Royal, Green Blue Fire, and green lookup tables were used to display septin-GFP signal. Computation, particle detection, and plot generation was performed using MATLAB software. For reliable detection of particles against noisy background, we used Guassian Mixture Modeling based particle detection algorithm from the MATLAB based u-track package (5). Each detected particle was characterized by the background level, particle amplitude above background, and particle radius. Automated tracking algorithm in the u-track package could not reliably track particles after the initial stages of assembly on supported lipid bilayers due to the high density of particles. Consequently, to quantify diffusion and length of septin particles, particles were manually tracked in ImageJ. To compare the intensity distribution of PH_{Num1}-mEGFP to septins in *S. pombe*, images of Spn1-mEGFP and PH_{Num1}-mEGFP were with acquired with identical settings and particles were detected using the same software described above (6).

Fluorescence Correlation Spectroscopy

Diffusion coefficient and brightness of septins labeled with mEGFP in solution and in the cytoplasm of fungal cells was determined using commercial PicoQuant hardware and software on a Nikon A1 LSM using a Plan Apo IR 60x WI 1.27NA objective. Identical laser intensity was used when comparing septins labeled with mEGFP to mEGFP in solution (Cell Sciences CRE131B) or to constitutively expressed mEGFP in the cytoplasm. In solution, fluctuations in fluorescence intensity were monitored for 1 minute; in cells signal was monitored for 10 seconds with lower laser intensity to prevent bleaching.

The autocorrelation function (ACF) obtained with afterpulsing suppression by means of fluorescence lifetime correlation spectroscopy (FLCS) with a pulsed laser (40 mHz) in SymPhoTime (PicoQuant GmbH, Germany) was fitted directly to a one component anomalous diffusion model in SymPhoTime:

$$G(\tau) = \frac{\gamma}{N}\left[1+\left(\frac{\tau}{\tau_D}\right)^{\alpha}\right]^{-1}\left[1+\frac{1}{\kappa^2}\left(\frac{\tau}{\tau_D}\right)^{\alpha}\right]^{-0.5}$$

where γ is a shape factor for the focal volume (1). For one photon excitation used here, $\gamma = 0.35$. N is the average number of molecules in the focal volume, τ_D is the diffusion time, α is the anomaly parameter, $\kappa = z_0 / w_0$ is the length to diameter ratio of the focal volume by approximating the shape of the focal volume by a Gaussian profile, with z_0 as the effective focal radius along the optical axis at $1/e^2$ intensity and w_0 as the effective lateral focal radius at $1/e^2$ intensity. $V_{eff} = \pi^{3/2} w_0^2 z_0$ is the effective excitation volume. The diffusion coefficient D is given by $D = w_0^2 / (4\tau_D)$. Fitting results from FCS

were exported to ASCII and imported to MATLAB (version 2011b, Mathworks) for plotting and statistical analysis.

The effective volume was calibrated by fitting the autocorrelation curve of 1.2 nM fluorescence dye Atto 488 in water (ATTO-TEC GmbH, Germany) to a triplet-state model

$$G(\tau)=\left(1-T+Te^{-\frac{\tau}{\tau_t}}\right)\frac{\gamma}{N}\left(1+\frac{\tau}{\tau_D}\right)^{-1}\left(1+\frac{\tau}{\kappa^2\tau_D}\right)^{-0.5}$$

Where T is the (triplet) fraction of molecules, τ_t is the life time of the triplet state. A length to diameter ratio of the focal volume $\kappa=5.15\pm0.35$ was obtained from the fitting. With the known diffusion coefficient D of Atto 488, the fitted τ_D from the autocorrelation curve, a confocal volume $V_{eff}=0.25\pm0.05$ fl was obtained.

Molecular brightness values were determined automatically by SymPhoTime software, independent of the fit, by dividing counts per second by the number of molecules in the optical volume.

Theoretical estimation of septin diffusivity as spheres and rods

Several considerations were made to model the behavior of septin complexes of a similar weight in either a rod or sphere arrangement. Assuming GFP is a sphere with mean protein density ρ, given the molecular weight m_w, the radius R is

$$R = \sqrt[3]{\frac{3m_w}{4\pi\rho N_A}}$$

Where N_A is Avagadro's constant and Stokes-Einstein relation gives

$$D = \frac{\kappa_B T}{6\pi\eta R}$$

Where D is the diffusion coefficient, κ_B is Boltzmann's constant, T is absolute temperature, η is viscosity. For rod-like molecules the diffusion coefficient D is given by

$$D = \frac{A\kappa_B T}{3\pi\eta L}$$

Where A is a correction factor defined as

$$A = \ln(L/d) + 0.312 + \frac{0.565}{L/d} - 0.1(L/d)^2$$

Where L is rod length and d is rod diameter (2).

The mean protein density ρ of a rod shape is related to its molecular weight by

$$\rho = \frac{m_w}{\pi(d/2)^2 L N_A}$$

Using the measured diffusion coefficient of GFP from FCS, assuming septins have the same mean protein density ρ as GFP and diffuse in the same viscosity and temperature, one can calculate theoretical diffusion coefficients of septins as spheres or

rods with different aspect ratio. For GFP, the molecular weight m_{GFP}=30 kDa was used, and for septin octamers in which Cdc11 is tagged with mEGFP, $m_{ws} = 443N$ kDa was used. For a septin rod with N end-on octamers, L=32N nm, and d=4nm.

Length Difference Pre-Annealing

1000 random pairs of annealing lengths were simulated using the observed distribution of particle lengths and the Kolmogorov-Smirnov (K-S) test was used to determine whether the difference in particle length at annealing was different than what would be expected by chance. Analyses and simulations were performed in R (version 2.15.1).

Persistence Length Measurements

Persistence length of septin filaments was determined using previously published methodology for actin and microtubules (3). Briefly, ten septin filaments with little length change over more than six frames (time interval 250 ms) were used to calculate persistence length. Two-dimensional coordinates (10-20 segments) were taken along the length of the septin filament. The filament shape was expressed as a superposition of Fourier modes with coefficient a_n. The mean variance of each mode is

$$\mathrm{var}(a_n) = < (a_n - a_n^0)^2 >$$

Where a_n^0 is the amplitude in the absence of applied or thermal forces. To account for variance by experiment noise ε_κ, the measured $\mathrm{var}(a_n)$ was fit to

$$\mathrm{var}(a_n)^{measured} = \left(\frac{L}{n\pi}\right)^2 \frac{1}{L_p} + (a_n^2)^{noise}$$

Where $$< a_n^2 >^{noise} = \frac{4}{L}\left(\varepsilon_\kappa^2\right)\left[1 + (N-1)\sin^2\left(\frac{n\pi}{2N}\right)\right]$$

The persistence length L_p for each mode is estimated from

$$\frac{1}{L_p} = \left(\frac{L}{n\pi}\right)^2\left[Var\left(a_n\right)^{measured} - \left(a_n^2\right)^{noise}\right]$$

Persistence length calculated from the first 5 modes for each filament was used to obtain a median value.

SI Figure Legends

Figure S1. Scheme of *S. cerevisiae* septin monomer, rod complex and elongated filament with Cdc11-mEGFP.

Figure S2. FCS of *S. cerevisiae* (AGY075, AGY115)*, S. pombe* (AGY093, AGY109) and *A. gossypii* (AG384.1, AG678.1). (A) Concentration of cytoplasmic septins as determined by fitting autocorrelation curves with an anamolous diffusion model. Concentrations are shown in nM. (B) Autocorrelation curves for purified Cdc11-mEGFP in solution and in the cytoplasm of *S. pombe* (Spn1-mEGFP), *S. cerevisiae*, and *A. gossypii* respectively. (C) Cytoplasmic *S. cerevisiae* Cdc11-mEGFP (AGY075) and Cdc3-mEGFP (AGY036) molecular brightness and diffusion constants compared to mEGFP (AGY115). Diffusion constants were determined by fitting autocorrelation curves with an anomolous diffusion model. (D) Cytoplasmic *A. gossypii* Cdc11a-mEGFP (AG384.1) molecular brightness and diffusion constants as determined by FCS. Diffusion constants were determined by fitting autocorrelation curves with an anomolous diffusion model.

Figure S3. Annealing on the cell cortex of *A. gossypii* monitored by TIRF microscopy.

Figure S4. Septins on supported lipid bilayers (A) Scheme of experimental design. Septins were placed on supported lipid bilayers and observed to form elongated structures over time. (B) Coomassie stain of purified septin complexes with Cdc11-mEGFP co-expressed in two bicistronic plasmids in *E. coli*. (C) Two dimensional diffusion of rhodamine labeled PE molecules in supported lipid bilayer. (D) Signal intensity at the supported lipid bilayer of different septin concentrations applied and measured over time. (E) Endpoint of 3 nM septin complexes added to plasma treated, BSA coated, and casein coated coverslips respectively. No filaments were observed.

Movie S1. Spn1-GFP particles moving and annealing on the cell cortex of *S. pombe* (AGY092). Note variability in brightness and size of particles. Acquired with 5 s intervals, displayed at 15 fps.

Movie S2. Annealing and fragmentation of Cdc11a-mEGFP filaments in hypha of *A. gossypii* cells (AG384.1). Acquired with 250 ms intervals, displayed at 15 fps.

Movie S3. Formation of Spn1-mEGFP septin ring by cortical annealing at the cell division plane of *S. pombe* (AGY093). Acquired with five second intervals, displayed at 20 fps.

Movie S4. Two dimensional diffusion of rhodamine-labeled phosphatidylethanolamine in supported lipid bilayers. Acquired with no delay between 100 ms exposures, displayed at 15 fps.

Movie S5. Purified septins (3 nM) assembling on bilayer. Acquired with 250 ms intervals, displayed at 15 fps.

Movie S6. Annealing event between septin particles on bilayer. Acquired with 250 ms intervals, displayed at 10 fps.

Movie S7. Cdc11-mEGFP septin filaments were assembled on bilayer, unbound complexes were washed out and Cdc11-mCherry complexes were added and monitored in TIRF. Acquired with 500 ms intervals, displayed at 15 fps.

Movie S8. Fragmentation and re-annealing of septin filaments on bilayer. Acquired with 250 ms intervals, displayed at 15 fps.

Movie S9. Cdc11-mEGFP septin filaments (1 nM) assembled on a supported lipid bilayer containing 4% DGS Ni-NTA. Acquired with 1 s intervals, displayed at 20 fps.

SI References

1. Schwille P, Haupts U, Maiti S, & Webb WW (1999) Molecular dynamics in living cells observed by fluorescence correlation spectroscopy with one- and two-photon excitation. *Biophysical journal* 77(4):2251-2265.
2. Tirado MM, Martinez CL, & Delatorre JG (1984) Comparison of Theories for the Translational and Rotational Diffusion-Coefficients of Rod-Like Macromolecules - Application to Short DNA Fragments. *J Chem Phys* 81(4):2047-2052.
3. Gittes F, Mickey B, Nettleton J, & Howard J (1993) Flexural rigidity of microtubules and actin filaments measured from thermal fluctuations in shape. *The Journal of cell biology* 120(4):923-934.
4. Schneider CA, Rasband WS, & Eliceiri KW (2012) NIH Image to ImageJ: 25 years of image analysis. *Nature methods* 9(7):671-675.
5. Jaqaman K*, et al.* (2008) Robust single-particle tracking in live-cell time-lapse sequences. *Nature methods* 5(8):695-702.
6. Zhang D, Vjestica A, Oliferenko & S (2012) Plasma Membrane Tethering of the Cortical ER Necessitates Its Finely Reticulated Architecture. *Current Biology* 22(21):2048-2052.

Figure S1

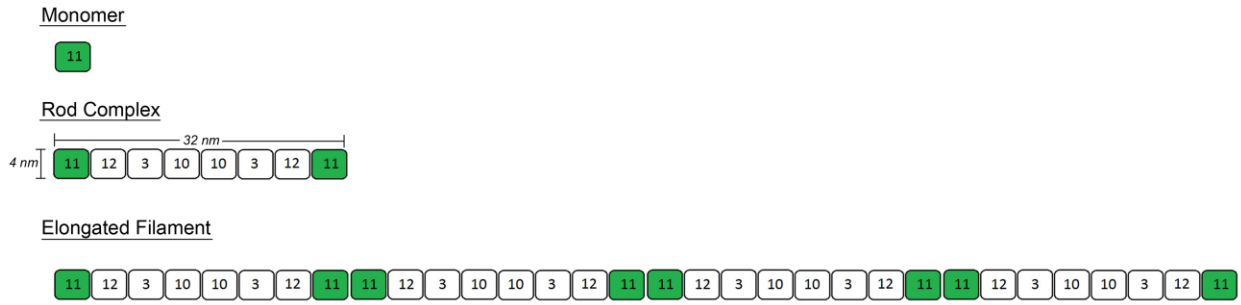
Monomer
11
Rod Complex
32 nm
4 nm
11 12 3 10 10 3 12 11
Elongated Filament
11 12 3 10 10 3 12 11 11 12 3 10 10 3 12 11 11 12 3 10 10 3 12 11 11 12 3 10 10 3 12 11

Figure S2

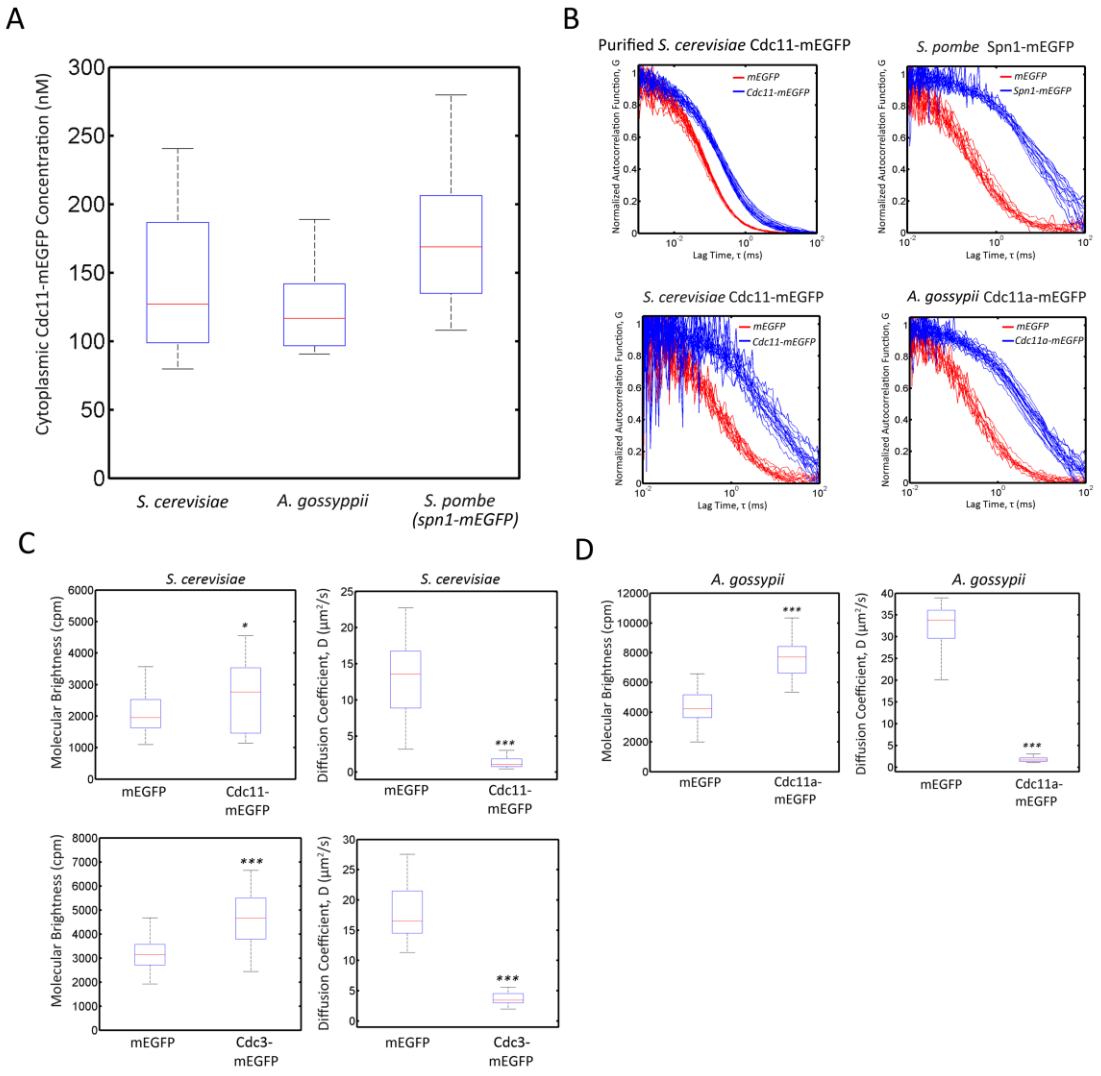
A
Cytoplasmic Cdc11-mEGFP Concentration (nM)
S. cerevisiae
A. gossyppii
S. pombe (spn1-mEGFP)
B
Purified S. cerevisiae Cdc11-mEGFP
S. pombe Spn1-mEGFP
S. cerevisiae Cdc11-mEGFP
A. gossypii Cdc11a-mEGFP
mEGFP
Cdc11-mEGFP
Spn1-mEGFP
Cdc11a-mEGFP
Normalized Autocorrelation Function, G
Lag Time, τ (ms)
C
S. cerevisiae
Molecular Brightness (cpm)
Diffusion Coefficient, D (μm²/s)
mEGFP
Cdc11-mEGFP
Cdc3-mEGFP
D
A. gossypii
Cdc11a-mEGFP

Figure S3

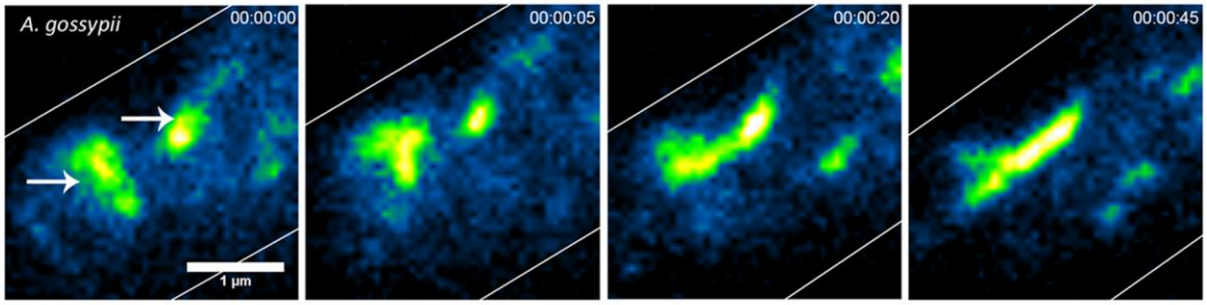

Figure S4